

Research Article

Precisely constrained 134-ka strong monsoon event in the penultimate deglaciation by an annually laminated speleothem from the Asian monsoon domain

Jiahui Cui^a, Jingyao Zhao^{a*}, Xiyu Dong^a , Carlos Pérez-Mejías^a , Jing Lu^a, Ye Tian^a , Jian Wang^a, Liangkang Pan^a, Haiwei Zhang^a  and Hai Cheng^{a,b,c}

^aInstitute of Global Environmental Change, Xi'an Jiaotong University, Xi'an 710049, China; ^bState Key Laboratory of Loess and Quaternary Geology, Institute of Earth Environment, Chinese Academy of Sciences, Xi'an 710061, China and ^cUniversal Scientific Education and Research Network (USERN), Xi'an, China

Abstract

The penultimate deglaciation was characterized by a sub-millennial-scale warm event in the Heinrich Stadial 11 (HS11), termed the 134-ka event. However, its precise timing and structure remain poorly constrained due to the lack of high-resolution and precisely dated records. We present an oxygen isotope record of a speleothem with well-developed annual lamina from Zhangjia Cave, located on the north margin of the Sichuan Basin, characterizing Asian summer monsoon (ASM) changes in the 134-ka event, which included an increase excursion of ca. 149 years and decrease excursion of ca. 200 years, inferred from 3.3‰ $\delta^{18}\text{O}$ variations. This event also divided the weak ASM interval-II (WMI-II), corresponding to HS11, into two stages, the WMI-IIa 132.8–134.1 ka and WMI-IIb 134.4–136.4 ka. With a comparable climatic pattern globally, the 134-ka event is essentially similar to the millennial-scale events in last glacial–deglacial period. Particularly, the observed weak-strong-weak ASM sequence (138.8–132.8 ka) is largely controlled by changes in the Atlantic Meridional Overturning Circulation (AMOC) forced by the meltwater of northern high-latitude ice sheets. Moreover, our results underpin that AMOC, rather than the global ice volume, is more critical to ASM variations during the last two deglaciations.

Keywords: Penultimate deglaciation, Asian summer monsoon, Heinrich Stadial 11, Speleothem $\delta^{18}\text{O}$ record

INTRODUCTION

The transition of the Earth's climate from full glacial to full interglacial conditions, known as the deglaciation process, is characterized by global warming and sea-level rising (ice sheet melting) (e.g., Denton et al., 2010; IPCC, 2013). During the penultimate deglaciation, massive iceberg discharges and the accompanying freshwater influx into the North Atlantic triggered a slowing or shutdown of the Atlantic Meridional Overturning Circulation (AMOC) (e.g., Grant et al., 2014; Tzedakis et al., 2018; Max et al., 2022). The reduced heat transport in the surface-ocean from the tropic to the North Atlantic resulted in the millennial-scale cooling stadial, namely Heinrich Stadial 11 (HS11), and the associated global effect.

Generally, deglaciations were often punctuated by millennial-scale events (e.g., Barker et al., 2009; Cheng et al., 2009, 2016) and/or significant variations in the AMOC (Marcott et al., 2011; Rasmussen et al., 2014; Cheng et al., 2016, 2021; Brook and Buizert, 2018; Ng et al., 2018; Toucanne et al., 2021). The large-scale climatic fluctuations that occurred during deglaciations are virtually an extension of the recurrence of millennial climatic variations during the glaci-als (e.g., the

Dansgaard–Oeschger [D-O] oscillations). Previous research has revealed that the D-O oscillations are closely associated with changes in the strength of the AMOC and corresponding changes in atmospheric circulation and sea ice coverage (e.g., Rasmussen and Thomsen, 2004; Dokken et al., 2013; Menviel et al., 2020).

One of the most studied D-O-like events in the last deglaciation is the Bølling–Allerød (B/A) warm period that occurred between ca. 14.7 and 12.9 ka (thousand years before present, where present = AD 1950) in the Northern Hemisphere (NH). This event began at the end of the cold period known as the HS1 and ended at the onset of the Younger Dryas (YD). Intriguingly, a similarly abrupt warm event occurred at ca. 134.5 ka (the 134-ka event) during the penultimate deglaciation, as inferred in the Asian summer monsoon (ASM) speleothem archives and Antarctic ice core records (e.g., Cheng et al., 2006; Wang et al., 2008).

The 134-ka event is a strong ASM interval centered at 134.5 ka in the penultimate deglaciation, characterized by a significantly negative oxygen isotope ($\delta^{18}\text{O}$) excursion in the speleothem records from the ASM domain (e.g., Cheng et al., 2006; Kelly et al., 2006; Wang et al., 2018; Duan et al., 2019). Atmospheric methane (CH_4) and nitrous oxide (N_2O) also show significant peaks at approximately 134 ka, as recorded in the European Project for Ice Coring in Antarctica (EPICA) Dome C (EDC) ice core records (Schmidely et al., 2021). The rise in CH_4 concomitant with the event also can be seen in the Vostok ice core record (Delmotte et al., 2004), and presumably resulted from the

*Corresponding author: Jingyao Zhao; Email: <zjy1230@xjtu.edu.cn>

Cite this article: Cui J et al (2024). Precisely constrained 134-ka strong monsoon event in the penultimate deglaciation by an annually laminated speleothem from the Asian monsoon domain. *Quaternary Research* 118, 116–125. <https://doi.org/10.1017/qua.2023.43>



expanded wetland due to enhanced tropical rainfall and temperature in NH (Bock et al., 2017). Additionally, contemporaneous hydroclimatic changes are widely reported in different proxy records from the North Atlantic region, including a short break in ice-rafted debris (IRD) deposition and a concomitant decrease in *N. pachyderma* abundance in marine sediments in the eastern subpolar North Atlantic (Martrat et al., 2014; Mokeddem et al., 2014; Tzedakis et al., 2018). On the other hand, the sea surface temperature (SST) fell at this time in the South Atlantic (the South Atlantic inversion) (Scussolini et al., 2015). Collectively, the co-occurrence of significant changes surrounding ca. 134 ka in different proxies in both hemispheres have delineated a large-scale sub-millennial climate event within HS11—the 134-ka event.

Since ~70% of the glacial–interglacial sea-level rise (i.e., meltwater pulse 2B [MWP-2B]) occurred during a phase of the weak AMOC (HS11) (Grant et al., 2012, 2014), the penultimate deglaciation fundamentally differed from the previous deglaciation (Marino et al., 2015). During the previous deglaciation, ~75% of the sea-level rise postdated the major deglacial cooling phase in the North Atlantic (HS1), and the largest meltwater pulse (MWP-1A, equivalent to 15–20% of the deglacial sea-level rise) peaked during the B/A warm period (Clark et al., 2002; Carlson and Clark, 2012). These observations fueled arguments that Antarctic ice sheets had contributed substantially to the MWP-1A (Clark et al., 2002). In contrast, the MWP-2B during the penultimate deglaciation was more than three times larger than the MWP-1A and was tied directly to circum-North Atlantic ice sheet reduction and attendant North Atlantic cooling (Marino et al., 2015).

This fundamentally different relationship between the North Atlantic climate and sea-level change during the two deglaciations indicates that during the penultimate deglaciation, NH ice sheets collapsed earlier in the deglaciation process, possibly in response to a combination of overall stronger (and more rapidly rising) boreal summer insolation and higher atmospheric CO₂ (Marino et al., 2015). Currently, it is not clear whether the 134-ka event exhibits any similarity in terms of structure and mechanisms to the B/A event in the last deglaciation. Whether the different meltwater pulses during the two deglaciations would have caused the apparent difference between the 134-ka event and the B/A event remains unclear as well. Likewise, the bottom of the Greenland ice records reaches only to the Eemian interglacial (Marine Isotopic Stages [MIS] 5e) (Rasmussen et al., 2014). As such, the Greenland ice records are not useful for understanding millennial-scale climate changes beyond MIS 5e (Rasmussen et al., 2014), including the 134-ka event, although a detailed characterization of the 134-ka event is critical to decipher the difference and link between the last two deglaciations, as well as the underlying causal mechanism(s).

In this study, we report a newly generated speleothem $\delta^{18}\text{O}$ record from Zhangjia Cave, southwestern China, ranging from 132.8 ± 0.3 ka to 138.8 ± 0.4 ka. On the basis of precise ^{230}Th dating and annual-lamina counting, we characterized the detailed structure of centennial climate events in the penultimate deglaciation, particularly the 134-ka event. The comparison/correlation of our Zhangjia record with records from a number of previous speleothems, ice-core records, and marine sediment records provides new constraints on the timing of the 134-ka event globally with unprecedentedly high-precision.

CAVE LOCATION AND STALAGMITE SAMPLE

Zhangjia Cave (32°35'N, 105°58'E, 680 m above sea level) is located at northeastern Guangyuan City, on the northern edge of the Sichuan Basin in the south of the Daba Mountains (Micang Mountains) (Fig. S1). The cave, formed in the limestones of the Lower Triassic Feixianguan Formation, has an entrance of $3 \times 4 \text{ m}^2$, and its total length exceeds 1 km (Fig. 1).

The columnar-shaped calcite stalagmite sample ZJD2020-1, which is 25.3 cm in height and ~6 cm in width (Fig. 2a), was collected in the first cave chamber, ~800 m from the cave entrance. Sample ZJD2020-1 was broken and scattered on the ground, which most likely was a result of an earthquake. According to instrumental data from the Guangyuan meteorological station (~54 km southwest of the cave), the mean annual air temperature is 16.1°C, and the mean annual precipitation is ~950 mm, ~74% of which occurs during summer (June to September) (1951–2019) (Fig. S1).

METHODS

^{230}Th dating

Subsamples of 20–60 mg were hand-drilled along growth layers for ^{230}Th dating. Eighteen powder subsamples were drilled from the polished slab of sample ZJD2020-1 using a carbide dental burr of 0.5 mm diameter (Table 1). The subsamples were dated using multi-collector inductively coupled plasma mass spectrometry (Neptune Plus, Thermo Scientific) in the Isotope Laboratory of Xi'an Jiaotong University. All errors are reported as two standard deviations (2σ). Standard chemistry procedures were used to separate U and Th (Edwards et al., 1987). A triple-spike (^{229}Th – ^{233}U – ^{236}U) isotope dilution method was employed to correct instrumental fractionation and determine U and Th isotopic ratios and concentrations. The instrumentation, standardization, and half-lives are reported in Cheng et al. (2000, 2013). All U/Th isotopes were measured in peak-jumping mode on a MasCom multiplier placed behind the retarding potential quadrupole. We followed procedures similar to those described in (Cheng et al., 2000) to characterize the multiplier. Uncertainties in U/Th isotopic data were calculated offline, including corrections for blanks, multiplier dark noise, abundance sensitivity, and spike composition. ^{230}Th ages were corrected using an initial $^{230}\text{Th}/^{232}\text{Th}$ atomic ratio of $(4.4 \pm 2.2) \times 10^{-6}$, the values for a material at secular equilibrium with respect to the bulk Earth $^{232}\text{Th}/^{238}\text{U}$ value of 3.8. The U and Th decay constants are reported in Jaffey et al. (1971) and Cheng et al. (2013).

Stable isotopes

For each oxygen isotope measurement, ~100 μg of powder samples were drilled from the central axis of the stalagmite. Subsamples (253 in total) were micro-milled at 1-mm increments perpendicular to the growth axes and analyzed using a Thermo Scientific MAT253 plus mass spectrometer coupled with an online carbonate preparation device (Kiel IV) at the Isotope Laboratory, Xi'an Jiaotong University, China. The results show an analytical error (1σ) for $\delta^{18}\text{O}$ of 0.06‰. International standards were added to the analysis every 10–20 samples to check reproducibility. The results are reported relative to the Vienna Pee Dee Belemnite (VPDB) standard in δ -notation (‰).

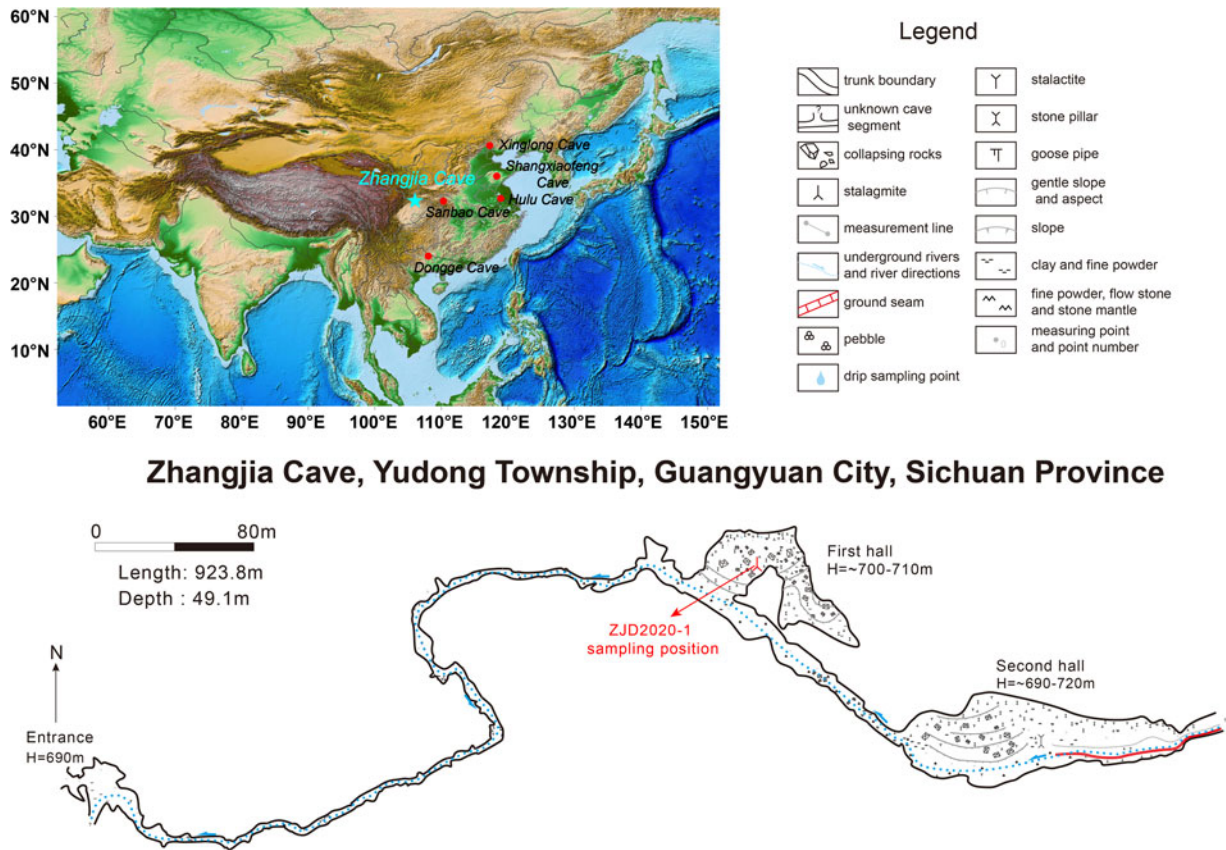


Figure 1. Location map and cave topographic map of Zhangjia Cave. The blue star depicts the studied cave (Zhangjia Cave). Red dots indicate cave records from the Asian monsoon domain. The cave topographic map of Zhangjia Cave is also shown.

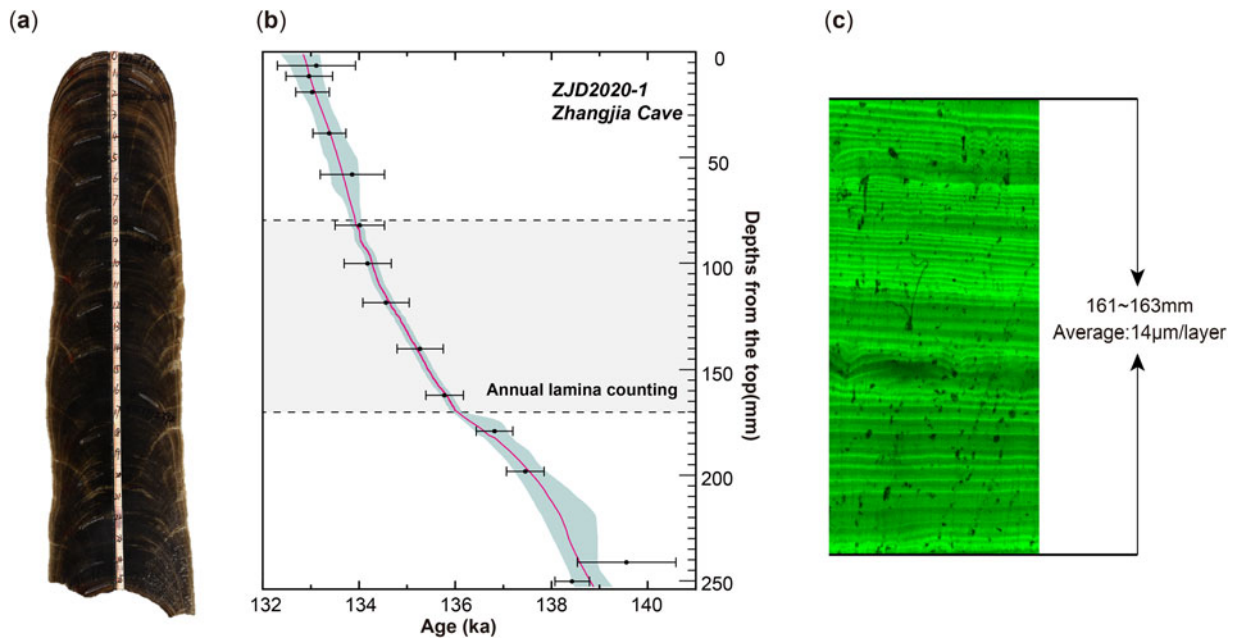


Figure 2. Age model of the studied speleothem record. (a) Stalagmite sample ZJD2020-1 (b) Age model of ZJD2020-1 from Zhangjia Cave. (c) Fluorescent lamina of ZJD2020-1 at 161~163 mm. Error bars show U-Th dates and errors (2σ). Age models were calculated combining the StalAge algorithm (Scholz and Hoffmann, 2011) and lamina counting.

Table 1. ^{230}Th dating results; 2σ error.

Sample Number	Depths (mm)	^{238}U (ppb)	^{232}Th (ppt)	$^{230}\text{Th}/^{232}\text{Th}$ (atomic $\times 10^{-6}$)	$^{230}\text{Th} / ^{238}\text{U}$ (activity)	$\delta_{\text{Initial}}^{234}$ (** (corrected))	^{230}Th Age (yr) (corrected)
ZJD2020-1-T	6.5	3295.2 \pm 5.0	120 \pm 9	343309 \pm 25406	0.7561 \pm 0.0015	90 \pm 3	133116 \pm 813
ZJD2020-1-2	11.5	4064.0 \pm 2.9	301 \pm 8	170814 \pm 4789	0.7673 \pm 0.0010	110 \pm 2	132965 \pm 484
ZJD2020-1-A2	19.0	6541.8 \pm 4.0	304 \pm 7	265726 \pm 6429	0.7481 \pm 0.0007	76 \pm 1	133032 \pm 348
ZJD2020-1-A3	38.5	7374.7 \pm 4.4	200 \pm 5	455081 \pm 12455	0.7472 \pm 0.0006	73 \pm 1	133385 \pm 342
ZJD2020-1-A4	58.0	9878.4 \pm 14.4	517 \pm 11	238023 \pm 5105	0.7557 \pm 0.0012	86 \pm 3	133862 \pm 666
ZJD2020-1-3	82.0	11986.8 \pm 12.8	177 \pm 7	849523 \pm 34974	0.7596 \pm 0.0010	92 \pm 2	134018 \pm 513
ZJD2020-1-A6	100.0	12083.6 \pm 11.5	116 \pm 3	1290758 \pm 35997	0.7529 \pm 0.0010	79 \pm 2	134181 \pm 489
ZJD2020-1-A7	118.5	11758.7 \pm 10.9	279 \pm 6	524248 \pm 11983	0.7542 \pm 0.0009	80 \pm 2	134560 \pm 482
ZJD2020-1-A8	140.0	9343.5 \pm 10.2	134 \pm 4	875149 \pm 25961	0.7602 \pm 0.0011	87 \pm 2	135271 \pm 479
ZJD2020-1-4	162.0	9488.1 \pm 6.5	255 \pm 8	467504 \pm 14293	0.7613 \pm 0.0008	86 \pm 1	135779 \pm 392
ZJD2020-1-A9	179.0	9806.0 \pm 6.3	276 \pm 6	450385 \pm 10391	0.7675 \pm 0.0007	92 \pm 1	136818 \pm 379
ZJD2020-1-A10	198.0	10447.0 \pm 7.2	113 \pm 3	1179021 \pm 33216	0.7762 \pm 0.0007	104 \pm 2	137457 \pm 391
ZJD2020-1-B	241.0	12541.6 \pm 29.6	1193 \pm 27	132957 \pm 3007	0.7671 \pm 0.0020	79 \pm 3	139560 \pm 1024
ZJD2020-1-A12	250.0	13171.0 \pm 8.7	3503 \pm 70	48440 \pm 971	0.7813 \pm 0.0007	109 \pm 1	138429 \pm 358

U decay constants: $\lambda_{238} = 1.55125 \times 10^{-10}$ (Jaffey et al., 1971) and $\lambda_{234} = 2.82206 \times 10^{-6}$ (Cheng et al., 2013). Th decay constant: $\lambda_{230} = 9.1705 \times 10^{-6}$ (Cheng et al., 2013). Corrected ^{230}Th ages assume the initial $^{230}\text{Th}/^{232}\text{Th}$ atomic ratio of $4.4 \pm 2.2 \times 10^{-6}$. Those are the values for a material at secular equilibrium, with the bulk earth $^{232}\text{Th}/^{238}\text{U}$ value of 3.8. The errors are arbitrarily assumed to be 50%.

* $d^{234}\text{U} = ((^{234}\text{U}/^{238}\text{U})_{\text{activity}} - 1) \times 1000$.

** $d^{234}\text{U}_{\text{Initial}}$ was calculated based on ^{230}Th age (T) (i.e., $\delta_{\text{Initial}}^{234} = \delta^{234}\text{U}_{\text{measured}} \times e^{\lambda_{234} \times T}$).

Fluorescent lamina study

The ZJD2020-1 sample was polished and scanned with a confocal laser fluorescence microscope (CLFM) (Model: Nikon, A1) at the State Key Laboratory of Mechanical Manufacturing Systems Engineering, Xi'an Jiaotong University. The image scanning was operated with a 40 mW, 488 nm laser line. The fluorescence images were obtained using an emission filter, which allows light with wavelengths of 505–550 nm (visible, green) to pass (Zhao and Cheng, 2017). The laminae counting was implemented in a section (82–170 mm) where laminae were quite clear. The results show an alternation between light and dark laminae with each light-dark pair corresponding to an annual growth cycle (Fig. 2c). Counts within the section (82–170 mm) were done for a total of five times. The laminae can be continuously identified, and the numbers of paired laminae between two consecutive ^{230}Th dates match the ^{230}Th age difference within uncertainty. This agreement supports our interpretation that the paired laminae indicate an annual cycle, which thus allows us to construct a precise relative age model.

RESULTS

Chronology

The 18 high-precision ^{230}Th dates (Table 1) obtained from the sample ZJD2020-1 were used to build the age model. The results show that sample ZJD2020-1 grew continuously from 132.8 ± 0.3 ka to 138.8 ± 0.4 ka (Table 1), covering the late portion of the penultimate glacial period. All dates are in stratigraphic order within errors (2σ), ranging from 327 yr to ca. 822 yr. The samples are clean, with high $^{230}\text{Th}/^{232}\text{Th}$ atomic ratios (0.04–1.2). The ^{238}U content is high (3–13 ppm), and the $\delta^{234}\text{U}_{\text{Initial}}$ values are approximately 127.

We used the least square method to anchor the results from annual band counting to the ^{230}Th dates (Domínguez-Villar et al., 2012), and establish a high-precision age model for the 82–170 mm section (Fig. 2c). In general, chronological models based on annual laminae counts are more accurate. In principle, there are two main sources of uncertainty associated with a floating chronology obtained by annual lamina counting: (A) lamina counting (LC) uncertainty (~ 113 [2σ] resulted from counting five times for ZJD2020-1), and (b) the uncertainty from anchoring (A) the LC chronologies to ^{230}Th dates (ca. 70 yr for ZJD2020-1). The combined error (ϵ) of annual-lamina counts in the 82–170 mm section is 132.5 yr (2σ), calculated by the following equation:

$$\epsilon = \sqrt{LC^2 + A^2}$$

The age models for the 0–82 mm and 170–253 mm segments were built using the StalAge Monte-Carlo simulation (Fig. 2c), and the 95% confidence limit was calculated from the distribution of the simulated fits (Scholz and Hoffmann, 2011). The ages are expressed in years before the present (AD 1950).

$\delta^{18}\text{O}$ and $\delta^{13}\text{C}$ records

The replication test between the ZJD2020-1 $\delta^{18}\text{O}$ record and different speleothem records suggests that the ZJD2020-1 $\delta^{18}\text{O}$ record reflects mainly large-scale regional precipitation $\delta^{18}\text{O}$ (Fig. 4), hence with insignificant influence from disequilibrium effects during carbonate precipitation. The ZJD2020-1 record contains ~ 253 $\delta^{18}\text{O}$ and $\delta^{13}\text{C}$ data points with a mean temporal resolution of ca. 24 yr. The $\delta^{18}\text{O}$ record spans 132.8–138.8 ka with $\delta^{18}\text{O}$ values ranging from -4.3‰ to -8.3‰ , with an average of -6.3‰ ,

and $\delta^{13}\text{C}$ data values varying between -6.2‰ to -10.2‰ . The $\delta^{18}\text{O}$ data recorded clear structures across a large portion of HS11, including the 134-ka event.

DISCUSSION

Interpretation of cave speleothem $\delta^{18}\text{O}$ and $\delta^{13}\text{C}$

Statistically significant negative correlations are seen between speleothem $\delta^{18}\text{O}$ values and rainfall amount proxies or wet/dry indexes from some regions in the ASM domain over the past ca. 60 yr (Zhang et al., 2018; Cheng et al., 2019; Zhao et al., 2019). Moreover, the results based on the Experimental Climate Prediction Center's Isotope-incorporated Global Spectral Model (IsoGSM) (Yoshimura et al., 2008) and water isotope-enabled Community Earth System Model (iCESM) (Hurrell et al., 2013) show a significant negative correlation between the simulated $\delta^{18}\text{O}$ of precipitation and rainfall amount on large regional scales (Fig. S2). IsoGSM and iCESM have been widely used for both modern and past climate simulations and have been proven to be in good agreement with observations of precipitation $\delta^{18}\text{O}$ from the Global Network of Isotopes in Precipitation (GNIP: <https://www.iaea.org/services/networks/gnip>) (Yoshimura et al., 2008). Additionally, the significant influence of upstream isotope depletion of $\delta^{18}\text{O}$ ("rainout effect") in East Asian speleothem $\delta^{18}\text{O}$ records was attributed to variations in the summer (southerly) monsoon wind (or spatial scales of the summer monsoon circulation) and related rainout-effect changes in the moisture trajectory (Pausata et al., 2011; Liu et al., 2014). In that regard, we suggest that the integrated oxygen isotopic fractionation from rainfall drives the $\delta^{18}\text{O}$ variability observed in the Zhangjia $\delta^{18}\text{O}$ record, including both rainfall at the cave site and in the upstream region of the moisture transport. The latter is sensitive to monsoon intensity, or the spatial scale of summer monsoon circulation, thus includes changes in the source of moisture. Recently, summer monsoon intensity as the main control of speleothem $\delta^{18}\text{O}$ variability in the ASM domain has been suggested (e.g., Cheng et al., 2016, 2019, 2022; Zhao et al., 2023). The consistency in the variations of the ASM speleothem $\delta^{18}\text{O}$ records on various timescales implies a common climatic control of the overall monsoon intensity (e.g., Cheng et al., 2012, 2016, 2019; Tan, 2014; Zhao et al., 2019; Liang et al., 2020). More broadly, the changes in large-scale monsoon circulation or monsoon intensity, including the moisture sources and integrated rainfall, would be the major factors affecting the speleothem $\delta^{18}\text{O}$ variation with large spatial consistency in ASM regions (e.g., Cheng et al., 2012, 2019; Zhao et al., 2019), corresponding to more (less) incorporated oxygen isotope fractionation of moisture from the remote (proximate) tropical oceanic sources to cave sites (e.g., Tan, 2014; Cheng et al., 2016, 2019).

Climate environment can affect the $\delta^{13}\text{C}$ values of stalagmites by one or several mechanisms, and the main controlling factors of $\delta^{13}\text{C}$ can vary with different historical periods and/or timescales. For example, $\delta^{13}\text{C}$ may reflect a variation of C3/C4 at glacial–interglacial timescales (Dorale et al., 1998; Denniston et al., 2013), but also may reflect variation of vegetation density and the yield of CO_2 at the millennial scale. Changes in the amplitude of temperature/precipitation at various timescales are main factors of the above phenomenon (Genty et al., 2003). In this study, we suggest that millennial-scale positive excursions in our $\delta^{13}\text{C}$ record are linked to increasing summer monsoon rainfall (Wang et al., 2018).

Two-stages of weak monsoon intervals

Our Zhangjia $\delta^{18}\text{O}$ record spans the weak monsoon interval-II (WMI-II) (Cheng et al., 2006, 2009; Kelly et al., 2006; Wang et al., 2018), which is characterized by higher $\delta^{18}\text{O}$ values with an average of approximately -5.8‰ . The Zhangjia record revealed two stages of the WMI-II: WMI-IIa (132.8–134.1 ka) and WMI-IIb (134.4–136.4 ka) (Fig. 4), separated by a short, strong ASM interval (134.1–134.4 ka). The WMI-IIa and WMI-IIb correspond to the cold events H11.2 and H11.1, respectively, as revealed by the cold stadials identified in the North Atlantic sediments (i.e., ice-rafted debris [IRD] events) recorded in cores MD03-2664 and ODP984 (Fig. 5i), benthic $\delta^{18}\text{O}$ events in core ODP 983, and U_{37}^k SST record in core MD01-2444 (Fig. 5e) (Channell et al., 1997; Mokeddem et al., 2014; Marino et al., 2015; Iralı et al., 2016; Tzedakis et al., 2018). Thus, the WMIs identified in the $\delta^{18}\text{O}$ record in southern China speleothems are presumably the counterparts of the low North Atlantic SST stadials (Jiménez-Amat and Zahn, 2015).

On the other hand, the North Atlantic stadials and Chinese WMIs coincide with a warming trend in the Southern Hemisphere, the increasing trend of atmospheric CO_2 and CH_4 (Petit et al., 1999; Cheng et al., 2016; Schmidely et al., 2021), and a southward shift and/or strengthening of the Southern Ocean westerlies (Toggweiler et al., 2006). The antiphase pattern between hemispheres is consistent with the "bipolar seesaw" (Stocker et al., 2003; Marino et al., 2015), which was accompanied by collapse of the AMOC (Deaney et al., 2017), a southward shift of the ITCZ (Jacobel et al., 2016), and ASM weakening (Cheng et al., 2016). In addition, the two stadials in NH appear to resemble the HS1 and YD (or HS0) during the last deglaciation, which apparently supports the assumption that the past two deglaciations are broadly similar in their structures (Cheng et al., 2009; Broecker et al., 2010).

Notably, the mean value of the Zhangjia $\delta^{18}\text{O}$ record is higher in the WMI-IIb (-5.1‰) than that in WMI-IIa (-6‰) (Fig. 5c), suggesting a weaker monsoon interval over the WMI-IIb in the penultimate deglaciation. This interval apparently correlates the North Atlantic stadial, as inferred by the low SST recorded both in the alkenone-based record in the ODP 976 core (Fig. 5d) from the Alboran Basin (Martrat et al., 2014) and the alkenone-based and Mg/Ca SST reconstructions from MD01-2444 core at the Iberian Margin (Fig. 5e) (Martrat et al., 2007, 2014; Tzedakis et al., 2018). These observations suggest an extremely cold H11.1 in H11, corresponding to an abrupt weakening of the ASM. However, this feature is not evident in some of the speleothem records from southern China. For instance, there is no obvious difference regarding the mean $\delta^{18}\text{O}$ values between WMI-IIa and WMI-IIb in the Dongge and Sanbao records (Fig. 4a, b). This discrepancy may be attributed to the regional differences in the ASM domain in response to the H11.1, which requires further investigation.

The 134-ka event during the penultimate deglaciation

One of the noticeable features of the Zhangjia $\delta^{18}\text{O}$ record is a centennial-scale abrupt strengthening of the ASM at 134.1–134.4 ka, which divides the WMI-II into two parts: the WMI-IIa and WMI-IIb (Fig. 4e). This strong ASM event, which is centered at 134.3 ± 0.13 ka, is constrained by the combination of the ^{230}Th dates and the fluorescence lamina counting results. This is consistent with the Hulu record, in which the

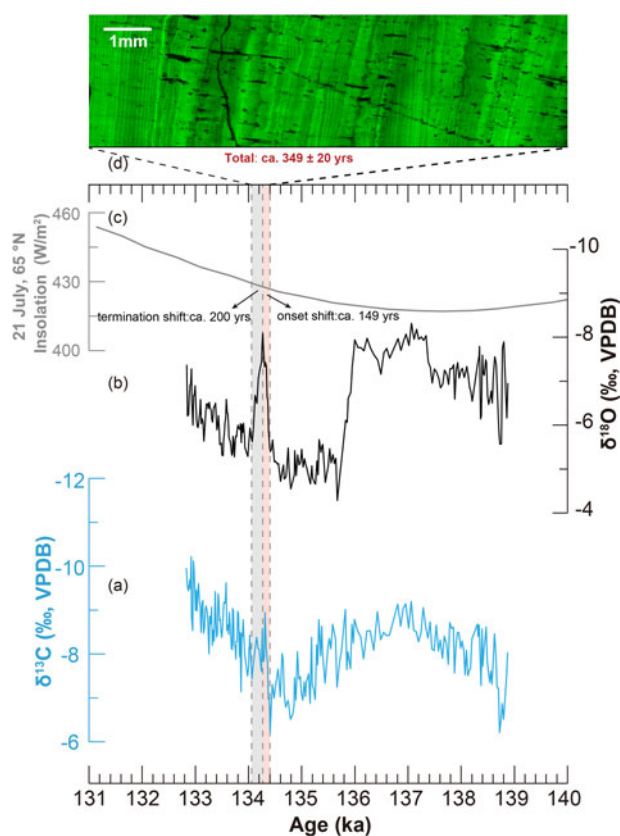


Figure 3. $\delta^{18}\text{O}$ and $\delta^{13}\text{C}$ records of Zhangjia Cave. From bottom to top: (a) ZJD2020-1 $\delta^{13}\text{C}$ record; (b) ZJD2020-1 $\delta^{18}\text{O}$ record. (c) Insolation at 65°N on 21 July. (d) Fluorescent lamina of ZJD2020-1 at 90–100 mm. Please note that the shifts in the 134-ka event shown on the Figure 3 have been calculated in the section of the stalagmite where lamina counting was conducted. This strong ASM event, which is centered at 134.3 ± 0.13 ka BP, is constrained by the combination of ^{230}Th dates and results of the fluorescence lamina counting.

corresponding strong ASM event occurred at 134.56 ± 1.0 ka, namely the Chinese Interstadial B.1 (CI B.1) (Cheng et al., 2006) (Fig. 4d). Based on our annual-lamina counting results of sample ZJD2020-1, the duration of the 134-ka event is 349 ± 20 yr. The onset of the event inferred by the $\delta^{18}\text{O}$ decrease ($\sim 3\text{‰}$) endures for ca. 149 yr, and the end of the event, which is inferred by the $\delta^{18}\text{O}$ increase ($\sim 3\text{‰}$), spans ca. 200 yr (Fig. 3). Our precise chronology confirms a previous notion that this event (or CI B.1) lasts no longer than several hundred years (Cheng et al., 2009). In the central and southern Chinese speleothem $\delta^{18}\text{O}$ records (Sanbao and Dongge records), the 134-ka event is also remarkable, although the amplitudes ($\sim 2\text{‰}$) are smaller than those in southwestern and northeastern China (Zhangjia and Hulu) ($\sim 3\text{‰}$) (Fig. 4). In addition, an abrupt negative excursion of the Zhangjia $\delta^{13}\text{C}$ ($\sim 3\text{‰}$) co-occurred at the onset of the 134-ka event inferred by the $\delta^{18}\text{O}$ change (Fig. 3a), suggesting an abrupt change of vegetation type/coverage and soil microbial activities in response to the onset of the event (Xue et al., 2019).

Climatic variations across the 134-ka event are also widely documented in a wide range of records in the North Atlantic region that are comparable to the ASM $\delta^{18}\text{O}$ records within age uncertainties; for example, the short cessation of IRD deposition with a concomitant decrease in *N. pachyderma* abundance in the ODP 984 core records from south of Iceland (Mokkeddem et al.,

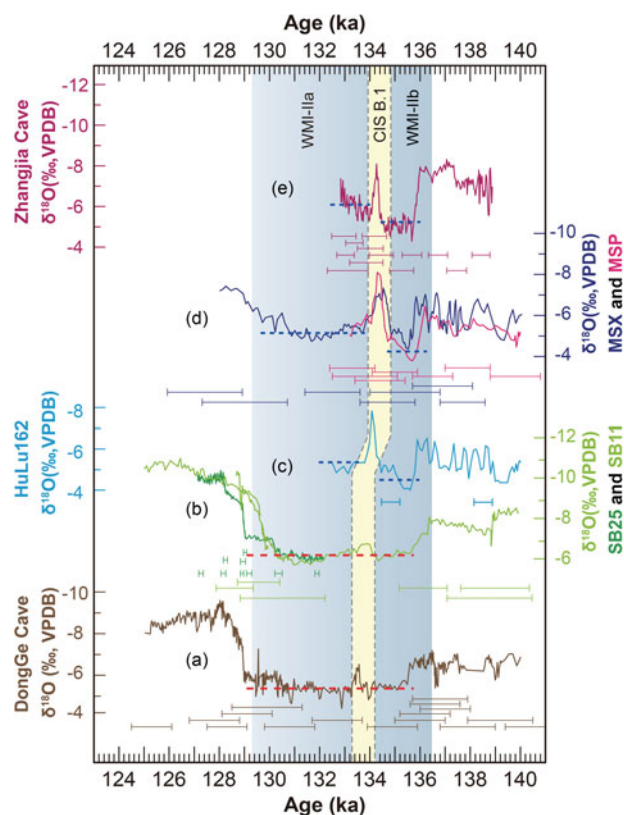


Figure 4. The 134-ka event in speleothem $\delta^{18}\text{O}$ from the ASM domain. From bottom to top: (a) $\delta^{18}\text{O}$ record from Dongge Cave speleothem D4 (Kelly et al., 2006); (b) speleothem SB-25 (dark green) and SB-11 (light green) $\delta^{18}\text{O}$ records from Sanbao Cave (Cheng et al., 2009); (c, d) speleothem HuLu162 (light blue), MSP (pink), and MSX (navy blue) $\delta^{18}\text{O}$ records from Hulu Cave (Cheng et al., 2006; Wang et al., 2018); (e) speleothem $\delta^{18}\text{O}$ record from Zhangjia Cave (this study). The ^{230}Th dates with uncertainties ($\pm 2\sigma$) are shown in each of the error bars. The vertical blue fields indicate weak monsoon intervals, and the vertical yellow interval indicates the 134-ka event. The horizontal red-dashed lines and blue-dashed lines represent the average levels of $\delta^{18}\text{O}$ during the time intervals. CIS = Chinese Interstadials.

2014; Tzedakis et al., 2018), the rise both in the alkenone-based SST in the ODP 976 core record (Fig. 5d) from the Alboran Basin (Martrat et al., 2014) and the Mg/Ca-based SST in the MD01-2444 core record from the Iberian Margin (Fig. 4e) (Martrat et al., 2007, 2014; Tzedakis et al., 2018). In the Southern Hemisphere, the SST in the South Atlantic dropped around the same time (the South Atlantic inversion), which is consistent with the “bipolar seesaw” scenario (Scussolini et al., 2015). Previously, the Vostok ice core methane (CH_4) record from Antarctica (Delmotte et al., 2004) showed a CH_4 peak near the 134-ka event. Recently, high-resolution records from the EPICA Dome C (EDC) ice-core in Antarctica (Schmidely et al., 2021) further characterized the significant CH_4 and nitrous oxide (N_2O) peaks at ca. 134.5 ka with durations similar to that in the Zhangjia $\delta^{18}\text{O}$ record (Fig. 5a, b). This abrupt increase in atmospheric CH_4 may be casually linked to the increased CH_4 emission due to enhanced tropical rainfall in the source regions (Bock et al., 2017), as well as NH temperature increase and monsoon intensification. Taken together, the 134-ka event has clear imprints in both hemispheres, with a global pattern similar to the D-O events, Greenland interstadials, and Chinese interstadials that are well defined in the last glacial–deglacial period (e.g., Cheng et al., 2006, 2009; Rasmussen et al., 2014; Tzedakis et al., 2018; Duan et al., 2019; Schmidely et al., 2021).

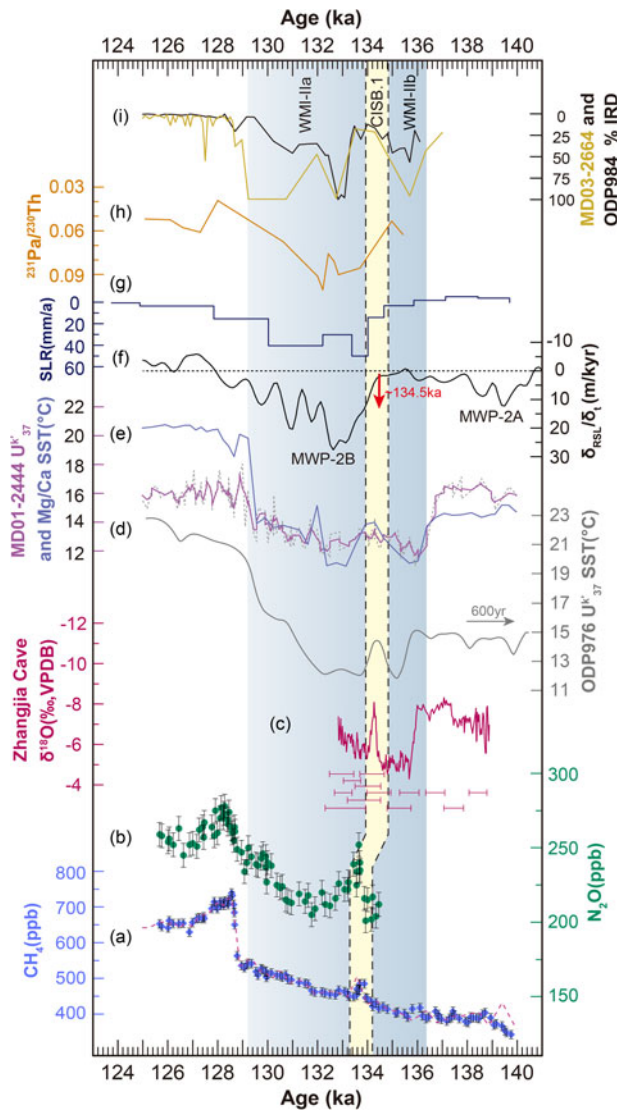


Figure 5. The 134-ka event in speleothem $\delta^{18}\text{O}$, marine-core, and Antarctic ice-core N_2O and CH_4 records. From bottom to top: (a) Antarctic EDC ice-core CH_4 record (Loulergue et al., 2008; Schmidely et al., 2021); (b) Antarctic EDC ice-core N_2O record (Schmidely et al., 2021); (c) speleothem $\delta^{18}\text{O}$ record from Zhangjia Cave (this study). The ^{230}Th dates with uncertainties ($\pm 2\sigma$) are shown in each of the error bars. (d, e) U_{57}^{235} SST from ODP 976 (gray) and U_{57}^{235} (purple) and Mg/Ca (gray blue) SST from MD01-2444 (Martrat et al., 2007, 2014; Tzedakis et al., 2018). (f) Freshwater fluxes calculated from rates of sea-level change (Grant et al., 2014); MWP = melt water pulse. (g) Global sea level rates from benthic $\delta^{18}\text{O}_{\text{benthic}}$ (Stoll et al., 2022); (h) Bermuda Rise $^{231}\text{Pa}/^{230}\text{Th}$ (Böhm et al., 2015). (i) IRD (ice-rafted debris) records from ODP984 (dark) (Mokkedem et al., 2014) and MD03-2664 (gold) (Irvali et al., 2016). The vertical blue fields indicate weak monsoon intervals, and the vertical yellow interval indicates the 134-ka event.

It is notable that while the durations of the 134-ka event are similar within age uncertainties among Zhangjia, Hulu, Dongge, and Sanbao speleothem $\delta^{18}\text{O}$ records, the event in the Xinglong and Shangxiaofeng speleothem $\delta^{18}\text{O}$ records appears to be much longer: >1600 yr (Fig. S3d; Duan et al., 2019) and ca. 1800 yr (Fig. S3e; Xue et al., 2019), respectively. This observation could imply a regional difference. However, given the broad consistency in terms of timing and structure of the CIs during the last glacial–deglacial period (e.g., Cheng et al., 2020; Li et al., 2020; Duan et al., 2022), it is likely that the sample resolution and age uncertainty of the Xinglong and Shangxiaofeng records

might partially explain the observed disparity. Additionally, the high-resolution CH_4 and N_2O records from the Antarctic EDC ice core records show a rather similar duration of a few hundred years for the 134-ka event (Fig. 5a, b), providing a strong constraint on the event duration globally. As such, we suggest that the unusually long duration of the apparent CIs around ca. 134 ka might be a unique feature in North China that resulted from the different regional climate response to the climate variations surrounding the event and/or sample resolution/dating uncertainty. Further studies are needed to resolve the discrepancy.

Climate dynamics underlying the 134-ka event

According to a common forcing mechanism for the deglaciation processes, the 134-ka event in the penultimate deglaciation, which is characterized by high amplitude and a short duration (300–400 yr) (Fig. 3), can be considered as a B/A-like event (B/A-II) in the last deglaciation. In contrast, the 134-ka event in the penultimate deglaciation had a much shorter duration (ca. 346 ± 20 yr) and smaller amplitude compared with the B/A interstadial in the last deglaciation. The B/A interstadial lasted more than 1800 yr (ca. 14.7 to 12.9 ka) (Fig. S4), during which the AMOC recovered to a level close to Holocene levels, as inferred by the $^{231}\text{Pa}/^{230}\text{Th}$ proxy from marine sediments (Fig. S4e) (Böhm et al., 2015). Although the 134-ka event occurred in the penultimate deglaciation with a much short duration compared with the B/A interstadial, the AMOC was also at a mode equivalent to that during the B/A interstadial, as inferred by the $^{231}\text{Pa}/^{230}\text{Th}$ record (Figure 5h) (Böhm et al., 2015). The end of the event might have been caused by a much larger freshwater forcing, the MWP-2B (Fig. 5f, g) (Schmidely et al., 2021; Stoll et al., 2022), which turned the AMOC to an “off” or “Heinrich” mode (Fig. 5h) (Böhm et al., 2015).

The MWP-2B, which is a major meltwater event during the penultimate deglaciation, contributed 70 m of sea-level rise (nearly 70% of the glacial–interglacial change) (Grant et al., 2012, 2014), with most meltwater discharged into the North Atlantic, as indicated by a large amount of IRD (Skinner and Shackleton, 2006; Grant et al., 2014; Marino et al., 2015). This ice sheet melting process broadly agrees with a large set of observations, such as reduction of the surrounding North Atlantic ice sheet and concomitant long-term cooling in the North Atlantic (Marino et al., 2015). On the other hand, the large MWP-2B apparently induced a long-term (ca. 5 ka) cold period, corresponding to the WMI-Ia (Fig. 5), which is much longer than the YD cold period (ca. 1.2 ka) in the last deglaciation (Fig. S4). Intriguingly, the MWP-1A, which was the largest meltwater pulse during the last deglaciation, occurred at an early stage of the B/A warm period (a strong ASM interval) and accounted for 15–20% of the deglacial sea-level rise mostly from Antarctic ice sheet meltwater (e.g., Weber et al., 2014). If the AMOC modes of the MWP-2B and MWP-1A periods are fundamentally different (Böhm et al., 2015), they correspond to weak and strong ASM, respectively (Cheng et al., 2009). These observations support the notion that ice volume is less effective in driving ASM changes (Cheng et al., 2022). In other words, the “ice volume effect” on the ASM would lie in its influence on the AMOC through North Atlantic meltwater forcing, and therefore the AMOC mode, not the ice volume, per se, would be more critical for low-latitude monsoons (Cheng et al., 2022). Additionally, the short duration (ca. 346 ± 20 yr) ASM event, the 134-ka event, appears to correlate with an abrupt AMOC change in a similar

duration. If so, this will call for modern work to further understand the large and fast switch of the AMOC mode on centennial timescales.

CONCLUSIONS

The Zhangjia high-resolution $\delta^{18}\text{O}$ record from southwestern China has provided unprecedented absolute and relative age precision, spanning 132.8–138.8 ka. This record precisely characterizes an abrupt ASM event, the 134-ka event, namely the CIS B.1 of previous Hulu records. The event occurred between 134.1–134.4 ka with a duration of ca. 349 ± 20 yr and $\delta^{18}\text{O}$ amplitude of $\sim 3\text{‰}$. As inferred by our $\delta^{18}\text{O}$ excursions, the onset of the 134-ka event endures for ca. 149 yr, and the end ca. 200 yr. This event separates the WMI-II in our record into two stages, WMI-IIa (132.8–134.1 ka) and WMI-IIb (134.4–136.4 ka). In comparison with North Atlantic climate records, we suggest that the 134-ka event, as a strong ASM event during the WMI-II that corresponded with the North Atlantic HS11, essentially corresponds to the millennial-scale events in the last glacial–deglacial period with a similar climatic pattern globally, including atmospheric CH_4 and N_2O jumps, the higher SST, and less IRD in the North Atlantic. It appears that the observed weak–strong–weak ASM rhythm from 138.8 ka to 132.8 ka in our record is largely controlled by the AMOC mode switches that were forced mainly by meltwater from northern high-latitude ice sheets. In this interpretative framework, the 134-ka event implies a centennial-scale faster AMOC mode or a break of the meltwater forcing in the North Atlantic, calling for further modeling study. Additionally, our results support the notion that the AMOC, rather than the ice volume, is more critical to ASM variations during deglacial processes.

Supplementary Material. The supplementary material for this article can be found at <https://doi.org/10.1017/qua.2023.43>

Acknowledgments. This study is supported by National Natural Science Foundation of China (NSFC 41888101, 42002199, and 42150710534).

REFERENCES

- Barker, S., Diz, P., Vautravers, M.J., Pike, J., Knorr, G., Hall, I.R., Broecker, W.S., 2009. Interhemispheric Atlantic seesaw response during the last deglaciation. *Nature* **457**, 1097–1102.
- Bock, M., Schmitt, J., Beck, J., Seth, B., Chappellaz, J., Fischer, H., 2017. Glacial/interglacial wetland, biomass burning, and geologic methane emissions constrained by dual stable isotopic CH_4 ice core records. *Proceedings of the National Academy of Sciences* **114**, E5778–E5786.
- Böhm, E., Lippold, J., Gutjahr, M., Frank, M., Blaser, P., Antz, B., Fohlmeister, J., Frank, N., Andersen, M.B., Deininger, M., 2015. Strong and deep Atlantic meridional overturning circulation during the last glacial cycle. *Nature* **517**, 73–76.
- Broecker, W.S., Denton, G.H., Edwards, R.L., Cheng, H., Alley, R.B., Putnam, A.E., 2010. Putting the Younger Dryas cold event into context. *Quaternary Science Reviews* **29**, 1078–1081.
- Brook, E.J., Buizert, C., 2018. Antarctic and global climate history viewed from ice cores. *Nature* **558**, 200–208.
- Carlson, A.E., Clark, P.U., 2012. Ice sheet sources of sea level rise and freshwater discharge during the last deglaciation. *Reviews of Geophysics* **50**, RG4007. <https://doi.org/10.1029/2011RG000371>.
- Channell, J.E.T., Hodell, D.A., Lehman, B., 1997. Relative geomagnetic paleointensity and $\delta^{18}\text{O}$ at ODP site 983 (Gardar Drift, North Atlantic) since 350 ka. *Earth and Planetary Science Letters* **153**, 103–118.
- Cheng, H., Edwards, R.L., Hoff, J., Gallup, C.D., Richards, D.A., Asmerom, Y., 2000. The half-lives of uranium-234 and thorium-230. *Chemical Geology* **169**, 17–33.
- Cheng, H., Edwards, R.L., Wang, Y., Kong, X., Ming, Y., Kelly, M.J., Wang, X., Gallup, C.D., Liu, W., 2006. A penultimate glacial monsoon record from Hulu Cave and two-phase glacial terminations. *Geology* **34**, 217–220.
- Cheng, H., Edwards, R.L., Broecker, W.S., Denton, G.H., Kong, X., Wang, Y., Zhang, R., Wang, X., 2009. Ice age terminations. *Science* **326**, 248–252.
- Cheng, H., Sinha, A., Wang, X., Cruz, F.W., Jr., Edwards, R.L., 2012. The global paleomonsoon as seen through speleothem records from Asia and the Americas. *Climate Dynamics* **39**, 1045–1062.
- Cheng, H., Lawrence Edwards, R., Shen, C.C., Polyak, V.J., Asmerom, Y., Woodhead, J., Hellstrom, J., et al., 2013. Improvements in ^{230}Th dating, ^{230}Th and ^{234}U half-life values, and U–Th isotopic measurements by multi-collector inductively coupled plasma mass spectrometry. *Earth and Planetary Science Letters* **371–372**, 82–91.
- Cheng, H., Edwards, R.L., Sinha, A., Spötl, C., Yi, L., Chen, S., Kelly, M., et al., 2016. The Asian monsoon over the past 640,000 years and ice age terminations. *Nature* **534**, 640–646.
- Cheng, H., Zhang, H., Zhao, J., Li, H., Ning, Y., Kathayat, G., 2019. Chinese stalagmite paleoclimate researches: a review and perspective. *Science China Earth Sciences* **62**, 1489–1513.
- Cheng, H., Xu, Y., Dong, X., Zhao, J., Li, H., Baker, J., Sinha, A., et al., 2021. Onset and termination of Heinrich Stadial 4 and the underlying climate dynamics. *Communications Earth & Environment* **2**, 230. <https://doi.org/10.1038/s43247-021-00304-6>.
- Cheng, H., Li, H., Sha, L., Sinha, A., Shi, Z., Yin, Q., Lu, Z., et al., 2022. Milankovitch theory and monsoon. *The Innovation* **3**, 100338. <https://doi.org/10.1016/j.xinn.2022.100338>.
- Clark, P.U., Mitrova, J., Milne, G., Tamisiea, M., 2002. Sea-level fingerprinting as a direct test for the source of global meltwater pulse 1A. *Science* **295**, 2438–2441.
- Deaney, E.L., Barker, S., van de Flierdt, T., 2017. Timing and nature of AMOC recovery across Termination 2 and magnitude of deglacial CO_2 change. *Nature Communications* **8**, 14595. <https://doi.org/10.1038/ncomms14595>.
- Delmotte, C., Chappellaz, J., Brook, E., Yiou, P., Barnola, J.-M., Goujon, C., Raynaud, D., Lipenkov, V., 2004. Atmospheric methane during the last four glacial–interglacial cycles: rapid changes and their link with Antarctic temperature. *Journal of Geophysical Research: Atmospheres* **109**, D12104. <https://doi.org/10.1029/2003JD004417>.
- Denniston, R.F., Asmerom, Y., Lachniet, M., Polyak, V.J., Hope, P., An, N., Rodzinyak, K., Humphreys, W.F., 2013. A last glacial maximum through Middle Holocene stalagmite record of coastal Western Australia climate. *Quaternary Science Reviews* **77**, 101–112.
- Denton, G.H., Anderson, R.F., Toggweiler, J.R., Edwards, R.L., Schaefer, J.M., Putnam, A.E., 2010. The last glacial termination. *Science* **328**, 1652–1656.
- Dokken, T.M., Nisancioglu, K.H., Li, C., Battisti, D.S., Kissel, C., 2013. Dansgaard–Oeschger cycles: interactions between ocean and sea ice intrinsic to the Nordic seas. *Paleoceanography* **28**, 491–502.
- Domínguez-Villar, D., Baker, A., Fairchild, I.J., Edwards, R.L., 2012. A method to anchor floating chronologies in annually laminated speleothems with U–Th dates. *Quaternary Geochronology* **14**, 57–66.
- Dorale, J.A., Edwards, R.L., Ito, E., Gonzalez, L.A., 1998. Climate and vegetation history of the Midcontinent from 75 to 25 ka: a speleothem record from Crevice Cave, Missouri, USA. *Science* **282**, 1871–1874.
- Duan, W., Cheng, H., Tan, M., Li, X., Edwards, R.L., 2019. Timing and structure of Termination II in north China constrained by a precisely dated stalagmite record. *Earth and Planetary Science Letters* **512**, 1–7.
- Edwards, R.L., Chen, J., Ku, T.-L., Wasserburg, G., 1987. Precise timing of the last interglacial period from mass spectrometric determination of thorium-230 in corals. *Science* **236**, 1547–1553.
- Genty, D., Blamart, D., Ouahdi, R., Gilmour, M., Baker, A., Jouzel, J., Van-Exter, S., 2003. Precise dating of Dansgaard–Oeschger climate oscillations in western Europe from stalagmite data. *Nature* **421**, 833–837.
- Grant, K.M., Rohling, E.J., Bar-Matthews, M., Ayalon, A., Medina-Elizalde, M., Ramsey, C.B., Satow, C., Roberts, A.P., 2012. Rapid coupling between

- ice volume and polar temperature over the past 150,000 years. *Nature* **491**, 744–747.
- Grant, K., Rohling, E., Ramsey, C.B., Cheng, H., Edwards, R., Florindo, F., Heslop, D., et al., 2014. Sea-level variability over five glacial cycles. *Nature Communications* **5**, 5076. <https://doi.org/10.1038/ncomms6076>.
- Hurrell, J.W., Holland, M.M., Gent, P.R., Ghan, S., Kay, J.E., Kushner, P.J., Lamarque, J.-F., et al., 2013. The community earth system model: a framework for collaborative research. *Bulletin of the American Meteorological Society* **94**, 1339–1360.
- IPCC (The Intergovernmental Panel on Climate Change) (Stocker, T.F., Qin, D., Plattner, G.-K., Tignor, M., Allen, S.K., Boschung, J., Nauels, A., Xia, Y., Bex, V., Midgley, P.M. [Eds.]), 2013. Climate Change 2013: The Physical Science Basis. Contribution of Working Group I to the Fifth Assessment Report of the Intergovernmental Panel on Climate Change. Cambridge University Press, Cambridge, UK, New York, 1535 pp.
- Irvali, N., Ninnemann, U.S., Kleiven, H.K.F., Galaasen, E.V., Morley, A., Rosenthal, Y., 2016. Evidence for regional cooling, frontal advances, and East Greenland Ice Sheet changes during the demise of the last interglacial. *Quaternary Science Reviews* **150**, 184–199.
- Jacobel, A.W., McManus, J.F., Anderson, R.F., Winckler, G., 2016. Large deglacial shifts of the Pacific intertropical convergence zone. *Nature Communications* **7**, 10449. <https://doi.org/10.1038/ncomms10449>.
- Jaffey, A.H., Flynn, K.F., Glendenin, L.E., Bentley, W.C., Essling, A.M., 1971. Precision measurement of half-lives and specific activities of ^{235}U and ^{238}U . *Physical Review C* **4**, 1889–1906.
- Jiménez-Amat, P., Zahn, R., 2015. Offset timing of climate oscillations during the last two glacial–interglacial transitions connected with large-scale freshwater perturbation. *Paleoceanography* **30**, 768–788.
- Kelly, M.J., Edwards, R.L., Cheng, H., Yuan, D., Cai, Y., Zhang, M., Lin, Y., An, Z., 2006. High resolution characterization of the Asian Monsoon between 146,000 and 99,000 years B.P. from Dongge Cave, China and global correlation of events surrounding Termination II. *Palaeogeography, Palaeoclimatology, Palaeoecology* **236**, 20–38.
- Li, Y., Rao, Z., Xu, Q., Zhang, S., Liu, X., Wang, Z., Cheng, H., Edwards, R.L., Chen, F., 2020. Inter-relationship and environmental significance of stalagmite $\delta^{13}\text{C}$ and $\delta^{18}\text{O}$ records from Zhenzhu Cave, north China, over the last 130 ka. *Earth and Planetary Science Letters* **536**, 116149. <https://doi.org/10.1016/j.epsl.2020.116149>.
- Liang, Y., Zhao, K., Edwards, R.L., Wang, Y., Shao, Q., Zhang, Z., Zhao, B., Wang, Q., Cheng, H., Kong, X., 2020. East Asian monsoon changes early in the last deglaciation and insights into the interpretation of oxygen isotope changes in the Chinese stalagmite record. *Quaternary Science Reviews* **250**, 106699. <https://doi.org/10.1016/j.quascirev.2020.106699>.
- Liu, Z., Wen, X., Brady, E.C., Otto-Bliesner, B., Yu, G., Lu, H., Cheng, H., et al., 2014. Chinese cave records and the East Asia Summer Monsoon. *Quaternary Science Reviews* **83**, 115–128.
- Loulergue, L., Schilt, A., Spahni, R., Masson-Delmotte, V., Blunier, T., Lemieux, B., Barnola, J.-M., Raynaud, D., Stocker, T.F., Chappellaz, J., 2008. Orbital and millennial-scale features of atmospheric CH_4 over the past 800,000 years. *Nature* **453**, 383–386.
- Marcott, S.A., Clark, P.U., Padman, L., Klinkhammer, G.P., Springer, S.R., Liu, Z., Otto-Bliesner, B.L., et al., 2011. Ice-shelf collapse from subsurface warming as a trigger for Heinrich events. *Proceedings of the National Academy of Sciences* **108**, 13415–13419.
- Marino, G., Rohling, E.J., Rodriguez-Sanz, L., Grant, K.M., Heslop, D., Roberts, A.P., Stanford, J.D., Yu, J., 2015. Bipolar seesaw control on last interglacial sea level. *Nature* **522**, 197–201.
- Martrat, B., Grimalt, J.O., Shackleton, N.J., de Abreu, L., Hutterli, M.A., Stocker, T.F., 2007. Four climate cycles of recurring deep and surface water destabilizations on the Iberian margin. *Science* **317**, 502–507.
- Martrat, B., Jimenez-Amat, P., Zahn, R., Grimalt, J.O., 2014. Similarities and dissimilarities between the last two deglaciations and interglaciations in the North Atlantic region. *Quaternary Science Reviews* **99**, 122–134.
- Max, L., Nürnberg, D., Chiessi, C.M., Lenz, M.M., Mulitza, S., 2022. Subsurface ocean warming preceded Heinrich Events. *Nature Communications* **13**, 4217. <https://doi.org/10.1038/s41467-022-31754-x>.
- Menviel, L.C., Skinner, L.C., Tarasov, L., Tzedakis, P.C., 2020. An ice–climate oscillatory framework for Dansgaard–Oeschger cycles. *Nature Reviews Earth & Environment* **1**, 677–693.
- Mokeddem, Z., McManus, J.F., Oppo, D.W., 2014. Oceanographic dynamics and the end of the last interglacial in the subpolar North Atlantic. *Proceedings of the National Academy of Sciences* **111**, 11263–11268.
- Ng, H.C., Robinson, L.F., McManus, J.F., Mohamed, K.J., Jacobel, A.W., Ivanovic, R.F., Gregoire, L.J., Chen, T., 2018. Coherent deglacial changes in western Atlantic Ocean circulation. *Nature Communications* **9**, 2947. <https://doi.org/10.1038/s41467-018-05312-3>.
- Pausata, F.S., Battisti, D.S., Nisancioglu, K.H., Bitz, C.M., 2011. Chinese stalagmite $\delta^{18}\text{O}$ controlled by changes in the Indian monsoon during a simulated Heinrich event. *Nature Geoscience* **4**, 474–480.
- Petit, J.R., Jouzel, J., Raynaud, D., Barkov, N.I., Barnola, J.M., Basile, I., Bender, M., et al., 1999. Climate and atmospheric history of the past 420,000 years from the Vostok ice core, Antarctica. *Nature* **399**, 429–436.
- Rasmussen, S.O., Bigler, M., Blockley, S.P., Blunier, T., Buchardt, S.L., Clausen, H.B., Cvijanovic, I., et al., 2014. A stratigraphic framework for abrupt climatic changes during the Last Glacial period based on three synchronized Greenland ice-core records: refining and extending the INTIMATE event stratigraphy. *Quaternary Science Reviews* **106**, 14–28.
- Rasmussen, T.L., Thomsen, E., 2004. The role of the North Atlantic Drift in the millennial timescale glacial climate fluctuations. *Palaeogeography, Palaeoclimatology, Palaeoecology* **210**, 101–116.
- Schmidely, L., Nehrbass-Ahles, C., Schmitt, J., Han, J., Silva, L., Shin, J., Joos, F., Chappellaz, J., Fischer, H., Stocker, T.F., 2021. CH_4 and N_2O fluctuations during the penultimate deglaciation. *Climate of the Past* **17**, 1627–1643.
- Scholz, D., Hoffmann, D.L., 2011. StalAge—an algorithm designed for construction of speleothem age models. *Quaternary Geochronology* **6**, 369–382.
- Scussolini, P., Marino, G., Brummer, G.-J.A., Peeters, F.J., 2015. Saline Indian Ocean waters invaded the South Atlantic thermocline during glacial termination II. *Geology* **43**, 139–142.
- Skinner, L., Shackleton, N., 2006. Deconstructing terminations I and II: revisiting the glacioeustatic paradigm based on deep-water temperature estimates. *Quaternary Science Reviews* **25**, 3312–3321.
- Stocker, T.F., Johnsen, S.J., 2003. A minimum thermodynamic model for the bipolar seesaw. *Paleoceanography* **18**, 1087. <https://doi.org/10.1029/2003PA000920>.
- Stoll, H.M., Cacho, I., Gasson, E., Sliwinski, J., Kost, O., Moreno, A., Iglesias, M., et al., 2022. Rapid northern hemisphere ice sheet melting during the penultimate deglaciation. *Nature Communications* **13**, 3819. <https://doi.org/10.1038/s41467-022-31619-3>.
- Tan, M., 2014. Circulation effect: response of precipitation $\delta^{18}\text{O}$ to the ENSO cycle in monsoon regions of China. *Climate Dynamics* **42**, 1067–1077.
- Toggweiler, J.R., Russell, J.L., Carson, S.R., 2006. Midlatitude westerlies, atmospheric CO_2 , and climate change during the ice ages. *Paleoceanography* **21**, PA2005. <https://doi.org/10.1029/2005PA001154>.
- Toucanne, S., Soulet, G., Vázquez Riveiros, N., Boswell, S.M., Dennielou, B., Waelbroeck, C., Bayon, G., et al., 2021. The North Atlantic glacial eastern boundary current as a key driver for ice-sheet–AMOC interactions and climate instability. *Paleoceanography and Palaeoclimatology* **36**, e2020PA004068. <https://doi.org/10.1029/2020PA004068>.
- Tzedakis, P.C., Drysdale, R.N., Margari, V., Skinner, L.C., Menviel, L., Rhodes, R.H., Taschetto, A.S., et al., 2018. Enhanced climate instability in the North Atlantic and southern Europe during the last interglacial. *Nature Communications* **9**, 4235. <https://doi.org/10.1038/s41467-018-06683-3>.
- Wang, Q., Wang, Y., Shao, Q., Liang, Y., Zhang, Z., Kong, X., 2018. Millennial-scale Asian monsoon variability during the late Marine Isotope Stage 6 from Hulu Cave, China. *Quaternary Research* **90**, 394–405.
- Wang, Y., Cheng, H., Edwards, R.L., Kong, X., Shao, X., Chen, S., Wu, J., Jiang, X., Wang, X., An, Z., 2008. Millennial- and orbital-scale changes in the East Asian monsoon over the past 224,000 years. *Nature* **451**, 1090–1093.
- Weber, M.E., Clark, P.U., Kuhn, G., Timmermann, A., Spreng, D., Gladstone, R., Zhang, X., et al., 2014. Millennial-scale variability in Antarctic ice-sheet discharge during the last deglaciation. *Nature* **510**, 134–138.

- Xue, G., Cai, Y., Ma, L., Cheng, X., Cheng, H., Edwards, R.L., Li, D., Tan, L., 2019. A new speleothem record of the penultimate deglacial: insights into spatial variability and centennial-scale instabilities of East Asian monsoon. *Quaternary Science Reviews* **210**, 113–124.
- Yoshimura, K., Kanamitsu, M., Noone, D., Oki, T., 2008. Historical isotope simulation using Reanalysis atmospheric data. *Journal of Geophysical Research* **113**, D19108. <https://doi.org/10.1029/2008JD010074>.
- Zhang, H., Cheng, H., Spötl, C., Cai, Y., Sinha, A., Tan, L., Yi, L., *et al.*, 2018. A 200-year annually laminated stalagmite record of precipitation seasonality in southeastern China and its linkages to ENSO and PDO. *Scientific Reports* **8**, 12344. <https://doi.org/10.1038/s41598-018-30112-6>.
- Zhao, J., Cheng, H., 2017. Applications of laser scanning confocal microscope to paleoclimate research: characterizing and counting laminae. *Quaternary Sciences* **37**, 1472–1474. [In Chinese]
- Zhao, J., Cheng, H., Yang, Y., Tan, L., Spötl, C., Ning, Y., Zhang, H., *et al.*, 2019. Reconstructing the western boundary variability of the Western Pacific Subtropical High over the past 200 years via Chinese cave oxygen isotope records. *Climate Dynamics* **52**, 3741–3757.
- Zhao, J., Cheng, H., Cao, J., Sinha, A., Dong, X., Pan, L., Pérez-Mejías, C., *et al.*, 2023. Orchestrated decline of Asian summer monsoon and Atlantic meridional overturning circulation in global warming period. *The Innovation Geoscience* **1**, 100011. <https://www.doi.org/10.59717/j.xinn-geo.2023.100011>.